2012

Structure and Magnetotransport Properties of Epitaxial Nanocomposite La0.67Ca0.33MnO3:SrTiO3 Thin Films Grown by a Chemical Solution Approach

Ling Fei

Leyi Zhu

Xuemei Cheng
Bryn Mawr College, xcheng@brynmawr.edu

Haiyan Wang

Stacy M. Baber

See next page for additional authors

Custom Citation
L. Fei *et al.*, *Appl. Phys. Lett.* **100**, 082403 (2012).

Authors
Ling Fei, Leyi Zhu, Xuemei Cheng, Haiyan Wang, Stacy M. Baber, Joshua Hill, Qianglu Lin, Yun Xu, Shuguang Deng, and Hongmei Luo

Structure and magnetotransport properties of epitaxial nanocomposite $La_{0.67}Ca_{0.33}MnO_3$:$SrTiO_3$ thin films grown by a chemical solution approach

Ling Fei,[1] Leyi Zhu,[2] Xuemei Cheng,[3,a)] Haiyan Wang,[4] Stacy M. Baber,[1] Joshua Hill,[1] Qianglu Lin,[1] Yun Xu,[1] Shuguang Deng,[1] and Hongmei Luo[1,a)]
[1]*Department of Chemical Engineering, New Mexico State University, Las Cruces, New Mexico 88003, USA*
[2]*Materials Science Division, Argonne National Laboratory, Argonne, Illinois 60439, USA*
[3]*Department of Physics, Bryn Mawr College, Bryn Mawr, Pennsylvania 19010, USA*
[4]*Department of Electrical and Computer Engineering, Texas A&M University, College Station, Texas 77843, USA*

(Received 15 October 2011; accepted 4 February 2012; published online 21 February 2012)

Epitaxial $La_{0.67}Ca_{0.33}MnO_3$:$SrTiO_3$ (LCMO:STO) composite thin films have been grown on single crystal $LaAlO_3$(001) substrates by a cost effective polymer-assisted deposition method. Both x-ray diffraction and high-resolution transmission electron microscopy confirm the growth of epitaxial films with an epitaxial relationship between the films and the substrates as $(002)_{film}||(002)_{sub}$ and $[202]_{film}||[202]_{sub}$. The transport property measurement shows that the STO phase significantly increases the resistivity and enhances the magnetoresistance (MR) effect of LCMO and moves the metal-insulator transition to lower temperatures. For example, the MR values measured at magnetic fields of 0 and 3 T are −44.6% at 255 K for LCMO, −94.2% at 125 K for LCMO:3% STO, and −99.4% at 100 K for LCMO:5% STO, respectively. © *2012 American Institute of Physics*. [doi:10.1063/1.3688048]

The colossal magnetoresistance (CMR) effect in perovskite rare-earth manganites $R_xA_{1-x}MnO_3$ (R is a rare-earth and A is a divalent cation) has triggered a great fundamental and practical interest in the past decades.[1–15] Its distinctive magnetic and electronic properties are considered to be related to the electron double exchange known as "DE" between mixed Mn^{3+} ($3d^4$)/Mn^{4+} ($3d^3$) ions and strong electron-phonon interactions arising from the John-Teller splitting of the Mn 3d level.[16] The grain boundaries, chemical disorder, oxygen deficiencies, and interfacial coupling have a strong impact on its ferromagnetic-paramagnetic and metal-insulator transition temperatures and the magnitude of the magnetoresistance (MR). $La_{0.67}Ca_{0.33}MnO_3$ (LCMO) based composite materials have been made by introducing an insulating second-phase into the LCMO matrix. For example, LCMO-SiO_2, LCMO-Mn_3O_4, LCMO-Al_2O_3, LCMO-polyphenylene sulfide (PPS), LCMO-$BaTiO_3$, LCMO-$SrTiO_3$, and LCMO-ZrO_2 have been reported.[3–12] In those bulk composites, the second-phase can tune and enhance the MR effect of LCMO. It is proposed that the enhanced magnetotransport occurs at the grain boundaries in polycrystalline manganites, and the insulating phase may produce additional spin-dependent scattering centers around the interfaces by increasing the magnetic nonuniformities and disorder.[10] However, it is not easy to control the grain boundaries in the bulk composite materials due to the ion diffusion, porosity, and poor grain connectivity.[15] Well-oriented epitaxial nanocomposite thin films can provide better control on the grain boundaries and great opportunities to tune the magnetotransport properties by introducing strain from the lattice mismatch between the films and substrates and the strain from the second-phase as well in the composites.[15,17–20] For example, greatly enhanced MR was reported in $La_{0.7}Ca_{0.3}MnO_3$:MgO nanocomposite films, which were coupled with phase transition and strain.[18]

Here, we report epitaxial nanocomposite LCMO:STO ($SrTiO_3$) films prepared by a polymer-assisted deposition (PAD) technique.[21,22] In the PAD process, the soluble polymer plays a significant role in the preparation of high-quality metal-oxide films; not only it controls the desired viscosity for the process but also binds the metal ions to prevent the premature precipitation. Thus, PAD provides a simple and straightforward way to prepare oxide composite materials.

The individual metal-polymer aqueous solution was prepared by binding metal ions (La^{3+}, Ca^{2+}, Mn^{4+}, Sr^{2+}, and Ti^{4+}) with polyethyleneimine (PEI, from Sigma-Aldrich, average $M_n \sim 60\,000$, $M_w \sim 750\,000$) and ethylenediaminetetraacetic acid (EDTA). Briefly, to prepare La, Ca, Mn, and Sr precursor solutions, 2 g EDTA and 2 g PEI were first dissolved in 40 mL water. Following that, 2 g $La(NO_3)_3 \bullet 6H_2O$, $Ca(OH)_2$, $MnCl_2 \bullet 4H_2O$, or $Sr(NO_3)_2$ were added to form a homogenous solution. For the Ti precursor solution, small aliquots of the titanium solution (made by slowly adding 2.5 g $TiCl_4$ to a mixture of 2.5 g of 30% hydrogen peroxide in 30 mL water) were added into the solution containing 1 g PEI, 1 g EDTA, and 30 mL water (maintaining the pH at 7.5). The solutions were separately filtered in an Amicon filtration unit that is designed to pass materials with molecular weight of less than 30 000 g/mol, to remove any unwanted unbound ions, and to concentrate the solution. The concentrations of La^{3+}, Ca^{2+}, Mn^{4+}, Sr^{2+}, and Ti^{4+} after such a filtration process were 125, 191, 148, 157, and 408 mM, respectively, as determined by inductively coupled plasma-atomic emission spectroscopy (ICP-AES). These solutions were mixed in the desired molar ratio needed to synthesize the single-phase LCMO and composite LCMO:STO films (molar ratios of LCMO:STO are 0.97:0.03, 0.95:0.05, and 0.90:0.10). These solutions were spin-coated onto $LaAlO_3$

a)Authors to whom correspondence should be addressed. Electronic addresses: xcheng@brynmawr.edu and hluo@nmsu.edu.

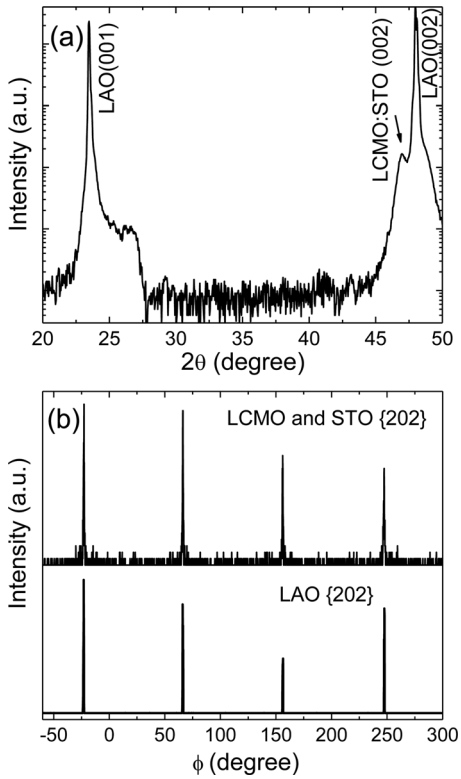

FIG. 1. XRD patterns of (a) θ-2θ scan of LCMO:5% STO film grown on LAO substrate; (b) ϕ-scans from (202) reflection of LCM:STO film and (202) of LAO substrate.

(LAO) substrates at 2000 rpm for 30 s. All the precursor films were annealed at 550 °C for 2 h to remove polymers and at 950 °C for 1 h in flowing oxygen to crystallize the oxides and achieve epitaxial growth of films. About 20 nm thick films were obtained from one spin-coat. X-ray diffraction (XRD) was used to characterize the crystal structure of the films. The surface morphology, microstructure, and the composition of the films was analyzed by scanning electron microscopy (SEM), high resolution transmission electron microscopy (HRTEM), and energy dispersive x-ray spectroscopy (EDS). The resistivity versus temperature characteristics were measured by a quantum design physical property measurement system (PPMS) along the film surface using a standard four-probe method, with the magnetic field applied normal to the film surface.

The lattice mismatch is 1.8% between LCMO and LAO, 1.2% between LCMO and STO, and 3% between STO and LAO, which were determined by considering the basal plane lattice parameters of LCMO ($a = 0.3858$ nm for pseudocubic perovskite unit cell), STO ($a = 0.3905$ nm), and LAO ($a = 0.3789$ nm). Such lattice mismatches make it possible to epitaxially grow both LCMO and STO on LAO substrates. All the single-phase LCMO and composite LCMO:STO films were investigated by the XRD analysis. It is noted that the XRD patterns of the composites are the same as those of the single phase LCMO on LAO. Fig. 1 shows the typical XRD θ-2θ and ϕ-scans of an LCMO:5% STO film on LAO substrate. As can be seen from the θ-2θ scan shown in Fig. 1(a), there are only (002) peak from the LCMO:5% STO film and (001) and (002) peaks from the LAO substrate. The only (002) peak appearing from the film indicates that the film is preferentially oriented along the c-axis, perpendicular to the substrate surface. According to the (002) peaks in the XRD pattern, the lattice parameter was calculated as $a = 0.3867$ nm for the LCMO:STO film and $a = 0.3791$ nm for the LAO. The (002) peak from LCMO may overlap with the (002) peak from STO because the lattice parameter of LCMO is close to that of STO. On the other hand, the (002) peak from STO may not appear since the STO concentration is too small in the composite. The in-plane orientation between the film and the substrate was determined by the XRD ϕ-scans from the (202) reflection from LCMO and STO and (202) from LAO. As shown in Fig. 1(b), four peaks 90° apart in the ϕ-scans indicate the four-fold symmetry of the cubic LCMO:STO film on the LAO substrate. An average full width at half-maximum (FWHM) value of 0.9° averaged from the four ϕ-scan peaks, in comparison with a value of 0.4° for the single-crystal substrate, indicates the films having a good epitaxial quality. Similar to LCMO on LAO substrate or LCMO on STO substrate,[19] the hetero-epitaxial relationships between the LCMO:STO composite films and the LAO substrate can be described as $(002)_{film}||(002)_{sub}$ and $[202]_{film}||[202]_{sub}$. Such epitaxial relationships can be easily understood by considering the crystal structure and the basal plane lattice parameters of LCMO, STO, and LAO.

The surface morphologies of the single-phase LCMO and LCMO:STO composite films are shown in Fig. 2. The labyrinth pattern with obvious boundaries is observed for the LCMO films. With the addition of STO, the grains grow bigger and the composite films are denser and smoother with no detectable micro-cracks. The cross-sectional HRTEM image of an LCMO:5% STO composite film on LAO substrate (Fig. 2(c)) confirmed the epitaxial relationship between the film and the substrate, which is consistent with the XRD analysis. The interface between the film and the substrate is flat and clean without any indication of intermixing. However, we could determine the LCMO phase but not the STO phase since the crystal structure of STO is very close to that of LCMO, and the STO concentration is too small. Sr, Ti, La, Ca, Mn, and O elements were confirmed by EDS analysis, as shown in Figs. 2(d) and 2(e). Because the Ti peaks are close to the La peaks (from both the sample and substrate), it is difficult to quantify the composition of the films. However, the amounts of Sr and Ti in LCMO:5% STO are obviously greater than those in LCMO:3% STO, as expected. It is noted that, by considering the ionic radius of Sr^{2+} (132 pm) and Ti^{4+} (74.5 pm), it is possible to form LCMO and STO solid solution by substituting Sr to La/Ca site (117.2 pm for La^{3+} and 114 pm for Ca^{2+}) and Ti to Mn site (72 pm for Mn^{3+} and 67 pm for Mn^{4+}). However, since we prepared precursor solution according to the compositions LCMO:STO (molar ratios of LCMO:STO are 0.97:0.03, 0.95:0.05, and 0.90: 0.10), the starting precursors are not $La_{0.67}Ca_{0.33-x}Sr_x$ $Mn_{1-x}Ti_xO_3$ ($x = 0.03$, 0.05, and 0.1). Therefore, we consider the system as compositions LCMO:STO, like LCMO:STO ceramic composites reported in Ref. 12 and LSMO:$BaTiO_3$ ceramic composites with 0, 1, and 5 mol. % $BaTiO_3$ in the composites in Ref. 23.

Figs. 3(a)–3(c) show the temperature (T)-dependent resistivity (ρ) of LCMO, LCMO:3% STO, and LCMO:5% STO composite films at different applied magnetic fields of

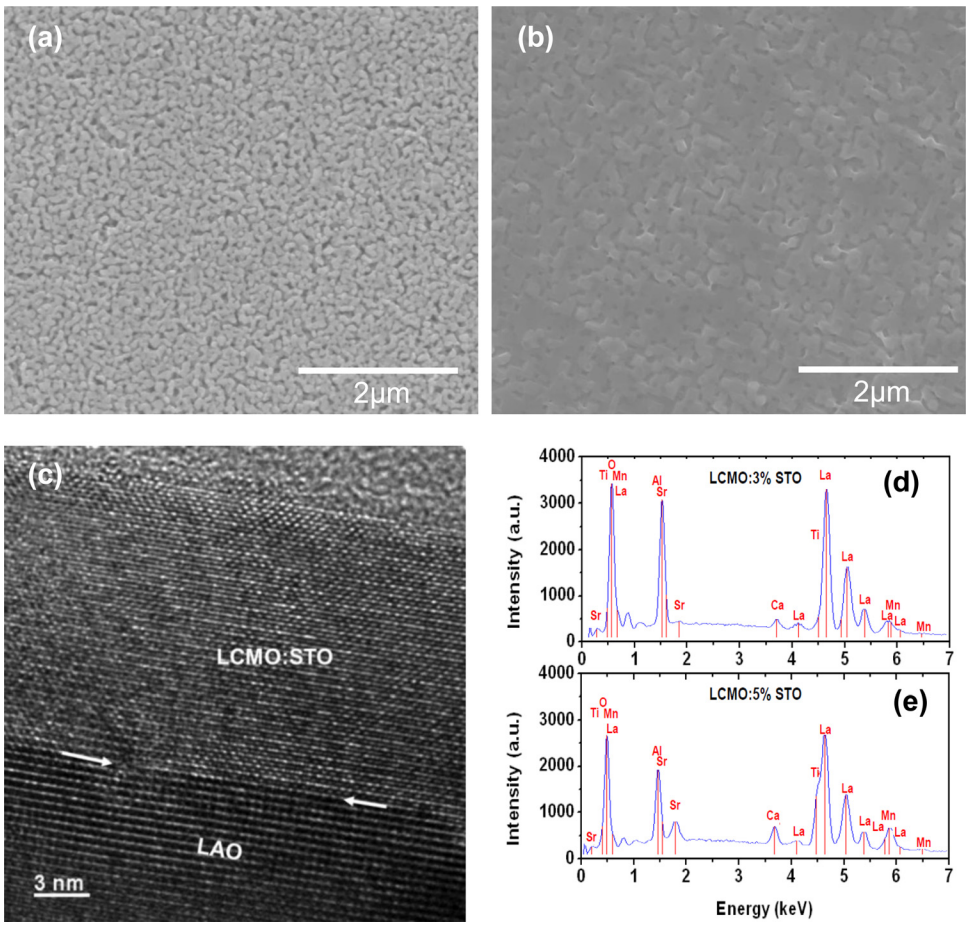

FIG. 2. (Color online) SEM images of LCMO (a), LCMO:5% STO (b), cross-section HRTEM image (c) of LCMO:5% STO films on LAO substrates, the EDS spectra of LCMO:3% STO (d), and LCMO:5% STO (e) on LAO substrates.

0 to 3 T. The metal-insulator-transition-like feature was observed with a peak temperature (T_p) in all the samples. However, the resistivity of the films increases significantly with the amount of STO. For example, the room-temperature resistivity at zero magnetic field increases from 0.0053 to 0.017 and 0.023 Ω•cm, and the maximum resistivity at T_p increases from 0.0061 to 0.3555 and 6.4163 Ω•cm for LCMO, LCMO:3% STO, and LCMO:5% STO, respectively.

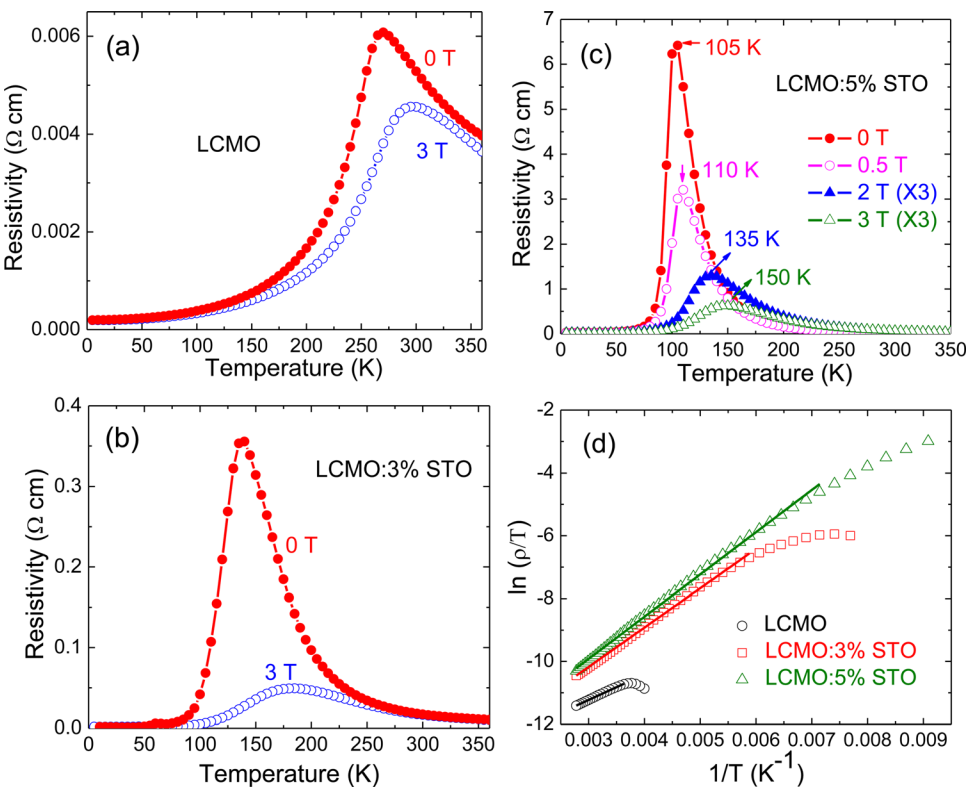

FIG. 3. (Color online) Temperature (T) dependent resistivity (ρ) of LCMO (a), LCMO:3% STO (b), and LCMO:5% STO (c) films at applied magnetic fields of 0, 0.5, 1, 2, and 3 T. (d)The experimental data (shown as symbols) and the linear fitting results (shown as solid lines) of $\ln(\rho/T) \sim 1/T$ for LCMO, LCMO:3% STO, and LCMO:5% STO films at temperatures higher than T_p and zero magnetic field.

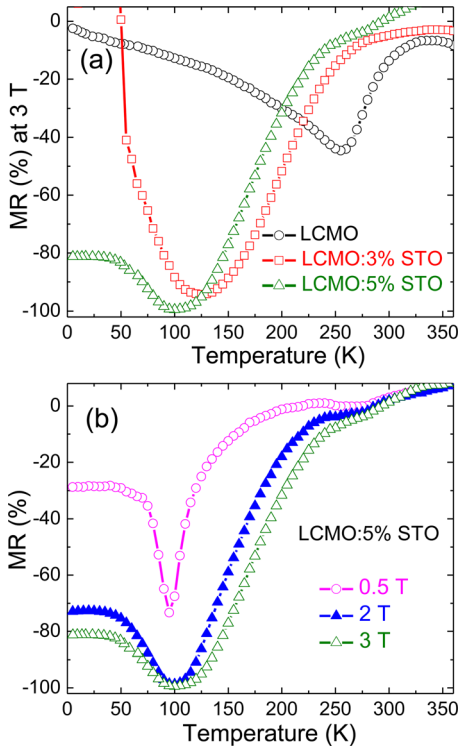

FIG. 4. (Color online) (a) The temperature dependent MR of LCMO, LCMO:3% STO, and LCMO:5% STO films at 3 T. (b) The temperature dependent MR of the LCMO:5% STO film at 0.5, 2, and 3 T.

This significant increase in resistivity is because the introduced insulating STO phase at the grain boundary obstructs the magnetic spin alignment near the grain boundary region of the manganite and, therefore, increases the tunneling barrier height between the neighboring magnetic grains.[24–27] The more the STO concentration is, the more significant the effect in increasing the tunneling barrier height is. In addition, the transition peak, T_p, shifts to lower temperatures as the STO concentration increases. This is also consistent with the obstruction of magnetic spin alignment near the grain boundary by the STO phase. To confirm the tunneling barrier height increase due to the STO phase, the $\rho(T)$ data above T_p were fitted with the adiabatic small polaron hopping model, $\rho = \rho_a T \exp[E_A/(k_B T)]$, where ρ_a is a constant, k_B is the Boltzmann constant, and E_A is the activation energy.[25] Therefore, $\ln(\rho/T) = \ln \rho_a + (E_A/k_B)(1/T)$ and in the $\ln(\rho/T) \sim 1/T$ plot (Fig. 3(d)), the slope is proportional to the activation energy E_A, representing the energy barrier height for spin-dependent hopping of electrons at the grain boundaries. Fig. 3(d) shows clearly that energy barrier height increases with addition of STO phase in the composite film.

On the other hand, the energy barrier height or activation energy decreases with applied magnetic field, resulting in lowering of resistance with applied magnetic field.[25] The observed dramatic decrease in resistivity with the applied 3 T magnetic field, as shown in Figs. 3(a)–3(c), indicates a strong MR effect. The transition peaks become wider and T_p shifts to a higher temperature as the magnetic field increases from 0 to 3 T. The MR values of these LCMO and LCMO:STO composites are calculated from the resistivity at magnetic fields of 0 and 3 T, MR $(\%) = (\rho_H - \rho_0)/\rho_0 \times 100$. As shown in Fig. 4(a), the maximum MR value at 3 T changed from −44.6% at 255 K for LCMO to −94.2% at 125 K for LCMO:3% STO and −99.4% at 100 K for LCMO:5% STO. The result clearly shows that we can tune the resistivity, maximum MR, and transition temperature of LCMO by adjusting the STO concentration in the composites. Fig. 4(b) shows the temperature dependence of the MR at different applied magnetic fields for LCMO:5% STO. The higher the magnetic field, the larger the magnitude of the MR. The MR values for our LCMO:STO composites are higher or comparable to those of other LCMO-based superlattice or composites, as seen from Table I. For example, the MR is −31% at 1 T and 77 K for LCMO:60% ZrO_2 composite,[9] −25% at 1.15 T and 93 K for LCMO:15% V_2O_5 composite,[13] −61% at 0.5 T and 109 K for LCMO:STO superlattice,[28] and −98% at 220 K and 6-7 T for superlattice LCMO:$Pr_{0.7}Ca_{0.30}MnO_3$.[29]

In summary, the epitaxial LCMO:STO composite thin films on LAO have been deposited by the polymer-assisted deposition. The STO phase increases the spin-dependent tunneling barrier height between the neighboring magnetic grains and therefore increases the resistivity. In addition, the STO phase changes the magnetoresistance dramatically by

TABLE I. The MR effects together with the transition temperature and magnetic fields of some LCMO single phase, doped LCMO, LCMO based superlattice and composites.

	Sample	H (T)	T (K)	MR (%)	Reference
	$La_{0.67}Ca_{0.33}MnO_3$	5	250	−88	1
	$La_{0.67}Ca_{0.33}MnO_3$	0.3	77	−17.75	14
	$La_{0.7}Ca_{0.3}MnO_3$	0.5	125	−38	25
Single phase	**$La_{0.67}Ca_{0.33}MnO_3$**	**3**	**255**	**−44.6**	This work
	$La_{0.7}Ca_{0.3}MnO_3$: $SrTiO_3$	0.5	109	−61	28
Superlattice	$La_{0.67}Ca_{0.33}MnO_3$:$Pr_{0.7}Ca_{0.30}MnO_3$	6–7	220	−98	29
	$La_{0.67}Ca_{0.33}MnO_3$:60%ZrO_2	1	77	−31	9
	$La_{0.67}Ca_{0.33}MnO_3$:15%V_2O_5	1.15	93	−25	13
	$La_{0.7}Ca_{0.3}MnO_3$: 3%$SrTiO_3$	**3**	**125**	**−94.2**	This work
		0.5	**95**	**−73.3**	
		2	**100**	**−98.6**	
Composite	**$La_{0.7}Ca_{0.3}MnO_3$: 5%$SrTiO_3$**	**3**	**100**	**−99.4**	This work
	$La_{0.67}Ca_{0.33}MnO_3$: 5%Cu	0.3	210	−50	30
Doping	$La_{0.67}Ca_{0.33}MnO_3$: 10%Co	6	100	−80	31

increasing the MR values and decreasing the metal-insulator transition temperatures, from 44.6% at 255 K for LCMO to −99.4% at 100 K for composite LCMO:5% STO.

Luo acknowledges the support from NSF/CMMI under Grant No. 1131290 and Interdisciplinary Research Grant (IRG) from NMSU. Cheng acknowledges the support from NSF/DMR under Grant No. 1053854. Wang acknowledges the support from NSF/DMR under Grant No. 1007969. This work was performed, in part, at the Center for Integrated Nanotechnologies, a U.S. Department of Energy, Office of Basic Energy Sciences user facility at Los Alamos National Laboratory (Contract DE-AC52-06NA25396) and Sandia National Laboratories (Contract DE-AC04-94AL85000).

[1]M. Jain, Y. Li, M. F. Hundley, M. Hawley, B. Maiorov, I. H. Campbell, L. Civale, and Q. X. Jia, Appl. Phys. Lett. **88**, 232510 (2006).
[2]M. Jain, P. Shukla, Y. Li, Mi. F. Hundley, H. Wang, S. R. Foltyn, A. K. Burrell, T. M. McCleskey, and Q. X. Jia, Adv. Mater. **18**, 2695 (2006).
[3]C. S. Xiong, Q. P. Huang, Y. H. Xiong, Z. M. Ren, L. G. Wei, Y. D. Zhu, X. S. Li, and C. L. Sun, Mater. Res. Bull. **43**, 2048 (2008).
[4]B. Vertruyen, R. Cloots, M. Ausloos, J. F. Fagnard, and Ph. Vanderbemden, Phys. Rev. B **75**, 165112 (2007).
[5]P. Phong, N. Khiem, N. Dai, D. Manh, L. Hong, and N. Phuc, Mater. Lett. **63**, 353 (2009).
[6]A. Gaur and G. Varma, Solid State Commun. **144**, 138 (2007).
[7]S. Keshri, L. Joshi, and S. K. Rout, J. Alloys Compd. **485**, 501 (2009).
[8]L. Joshi, S. S. Rajput, and S. Keshri, Phase Transitions **83**, 482 (2010).
[9]B. X. Huang, Y. H. Liu, R. Z. Zhang, X. B. Yuan, C. J. Wang, and L. M. Mei, J. Phys. D: Appl. Phys. **36**, 1923 (2003).
[10]A. Casaca, R. P. Borges, P. Ferreira, A. Saraiva, M. A. Rosa, R. C. da Silva, W. C. Nunes, S. Magalhães, and M. Godinho, J. Phys.: Conf. Ser. **153**, 012045 (2009).
[11]S. Liang, J. R. Sun, J. Wang, and B. G. Shen, Appl. Phys. Lett. **95**, 182509 (2009)
[12]D. K. Petrov, L. Krusin-Elbaum, J. Z. Sun, C. Field, and P. R. Duncombe, Appl. Phys. Lett. **75**, 995 (1999).
[13]S. Karmakar, S. Taran, B. K. Chaudhuri, H. Sakata, C. P. Sun, C. L. Huang, and H. D. Yang, J. Phys. D: Appl. Phys. **38**, 3757 (2005).
[14]H. K. Singh, N. Khare, P. K. Siwach, and O. N. Srivastava, J. Phys. D: Appl. Phys. **33**, 921 (2000).
[15]Z. X. Bi, E. Weal, H. M. Luo, A. P. Chen, J. L. MacManus-Driscoll, Q. X. Jia, and H. Y. Wang, J. Appl. Phys. **109**, 054302 (2011).
[16]C. Zener, Phys. Rev. **82**, 403 (1951).
[17]B. S. Kang, H. Wang, J. L. MacManus-Driscoll, Y. Li, Q. X. Jia, I. Mihut, and J. B. Betts, Appl. Phys. Lett. **88**, 192514 (2006).
[18]V. Moshnyaga, B. Damaschke, O. Shapoval, A. Belenchuk, J. Faupel, O. I. Lebedev, J. Verbeeck, G. Van Tendeloo, M. Mücksch, V. Tsurkan, R. Tidecks, and K. Samwer, Nature Mater. **2**, 247 (2003).
[19]C. J. Lu, Z. L. Wang, C. Kwon, and Q. X. Jia, J. Appl. Phys. **88**, 4032 (2000).
[20]A. P. Chen, Z. X. Bi, H. Hazariwala, X. H. Zhang, Q. Su, L. Chen, Q. X. Jia, J. L. MacManus-Driscoll, and H. Y. Wang, Nanotechnology **22**, 315712 (2011).
[21]Q. X. Jia, T. M. McCleskey, A. K. Burrell, Y. Lin, G. E. Collis, H. Wang, A. D. Q. Li, and S. R. Foltyn, Nature Mater. **3**, 529 (2004).
[22]A. K. Burrell, T. M. McCleskey, and Q. X. Jia, Chem. Commun. **11**, 1271 (2008).
[23]Z. Y. Zhou, G. S. Luo, and F. Y. Jiang, J. Magn. Magn. Mater. **321**, 1919 (2009).
[24]Y.-M. Kang, H.-J. Kim, and S.-I. Yoo, Appl. Phys. Lett. **95**, 052510 (2009).
[25]M. Staruch, D. Hires, A. Chen, Z. Bi, H. Wang, and M. Jain, J. Appl. Phys. **110**, 113913 (2011).
[26]Y. Lu, X. W. Li, G. Q. Gong, G. Xiao, A. Gupta, P. Lecoeur, J. Z. Sun, Y. Y. Wang, and V. P. Dravid, Phys. Rev. B **54**, R8357 (1996).
[27]P. Kameli1, H. Salamati, M. Eshraghi, and M. R. Mohammadizadeh, J. Appl. Phys. **98**, 043908 (2005).
[28]C. Kwon, K. C. Kim, M. C. Robson, J. Y. Gu, M. Rajeswari, T. Venkatesan, and R. Ramesha, J. Appl. Phys. **81**, 4950 (1997).
[29]A. Venimadhav, M. S. Hegde, R. Rawatb, I. Dasb, and M. E. Marssic, J. Alloys Compd. **326**, 270 (2001).
[30]C. S. Xiong, Y. B. Pi, Y. H. Xiong, Y. T. Mai, H. L. Pi, Z. M. Ren, J. Zhang, X. W. Cheng, L. Zhang, Y. D. Zhu, X. S. Li, Q. P. Huang, L. G. Wei, and W. Xu, J. Phys. D: Appl. Phys. **40**, 3531 (2007).
[31]N. Gayathri, A. K. Raychaudhuri, S. K. Tiwary, R. Gundakaram, A. Arulraj, and C. N. R. Rao, Phys. Rev. B **56**, 1345 (1997).